DAMPING OF FLEXURE BLADES BASED ON BI-MATERIAL ADDITIVE MANUFACTURING: OPPORTUNITY FOR NEW DAMPER TOPOLOGIES?

Lisa Salamin [(1)], Hervé Saudan [(1)], Lionel Kiener [(1)], Elias Klauser [(1)], Nicolas Blondiaux [(1)], Florent Boudoire [(1)], Nikola Kalentics [(1)], Olivier Rousseaux [(1)], Johanna Zikulnig [(2)]

[(1)] CSEM SA, Jaquet-Droz 1, 2002 Neuchâtel, Switzerland, Email: lisa.salamin@csem.ch
[(2)] Silicon Austria Labs GmbH, 9524 Villach, Austria, Email: johanna.zikulnig@silicon-austria.com

KEYWORDS

Flexure-based Mechanisms, Compliant Mechanisms, Bi-material Additive Manufacturing, Damping, Elastomer, Vibrations, Precision Mechanisms

ABSTRACT

In space applications, mechanisms and instruments are submitted to shocks and vibrations resulting from the rocket launch and other subsystems during operation. These harsh environmental conditions induce a need for damping systems to isolate the space mechanisms from disturbances. To tackle this challenge and preserve the friction-free properties of compliant mechanisms, CSEM added a damping action to their flexure-based technology. Damped flexure blades based on bi-material additive manufacturing were developed and validated. The blades consist of a sandwich of two planar parallel metallic lattice patterns with an elastomer impregnated in-between. These blades were characterized under free and forced sinusoidal oscillations. Compared with reference flexures, the damped flexures show quality factors Q reduced by a factor of 64. This reduction implies a damping action increased by a factor of 97 considering the viscous damping coefficient. These results open promising perspectives to develop new types of dampers.

1. INTRODUCTION

A key requirement of any space mechanism is to withstand vibrations and shocks resulting from the rocket launch (or landing), and the commissioning of the payload. Additionally, during operation, a space mechanism can be exposed to micro-vibrations produced by other subsystems (e.g., cryocoolers and reaction wheels). These micro-vibrations can affect the mechanism performance and, consequently, those of the instrument containing it [1]. The need for robust and reliable damping systems is therefore of great importance [2].

A well-known technology developed at CSEM is based on flexible elements in mechanisms that bend to allow the desired motion. Flexure-based motions comprehend numerous advantages for space applications. Indeed, the flexures exhibit high lifetime performance considering material fatigue. They can perform high-precision strokes for long periods of time as their deformations remain in the elastic domain. For instance, as shown in Fig. 1, the IASI Corner Cube Mechanism developed at CSEM to operate in European meteorological satellites METOP achieved 1.2 billion of cycles in 15 years [3]. Moreover, no solid friction is observed in these flexure-based mechanisms allowing cleanliness and wear-free motion [4]. Another advantage of such mechanisms is the possibility to manufacture them using additive manufacturing (AM) techniques. AM, in addition to be more eco-friendly [5], increases the design freedom and reduces the number of parts to assemble [6]. Thereby, adding damping to flexures allows decreasing the flexures sensitivity to vibrations while keeping their many advantages for space applications [2].

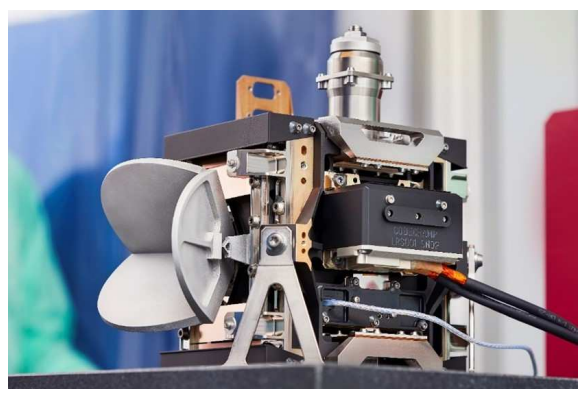

Figure 1: Corner Cube Mechanism Flight Model [7].

Flexure elements can be shaped and arranged in a wide range of topologies to achieve a variety of motion types, e.g., one rotational or linear stroke or a combination of them. As an example, Fig. 2 illustrates the possible motion obtained with two different types of blades.

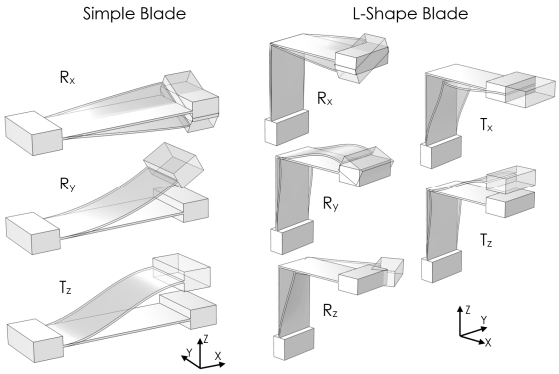

Figure 2: DOF of the simple blade (left) and the L-Shape blade (right).

Improving flexures with a damping capability would then increase the scope of their applications and open promising opportunities to develop new topologies for spring dampers. Indeed, any motion could be obtained by combining different flexure elements and hence the damper design could be precisely tailored to the desired application.

To damp a flexure blade, a solution consists in adding an elastomer that will deform with the flexure in operation. Indeed, as elastomers show viscoelastic properties, they dissipate significant energy when subjected to cyclic stress. This characteristic results from the molecular motion inside the elastomer that induces internal friction. As opposed to elastic materials which return nearly all the energy injected, elastomers exhibit a hysteresis behavior where part of the strain energy is dissipated into heat [8-9]. CSEM patented such a concept for small size mechanical components [10]. Its applicability to centimeter-scaled flexures is nevertheless nearly impossible, due to difficulty in adding the viscoelastic material in areas having low accessibility.
To overcome this problem, CSEM proposed to take advantage of AM to design and produce a *lattice flexure* (instead of a normal flexure) which is split into two blades. A small gap lies between them. Unlike normal flexures, the latter can be easily impregnated with a viscoelastic material in a liquid phase which flows to fill all voids between the two blades and solidifies [2].

In 2021, a proof of concept was additively manufactured and impregnated with a poly-urethane material. During preliminary tests in free oscillation mode, encouraging results have been obtained. To assess the performances of such a passive system more in depth, the need for further investigations was highlighted and is at the origin of the project detailed in this article.

2. METHODOLOGY

The methodology followed during this multidisciplinary project can be separated into four phases: the flexures design, the flexures manufacturing and impregnation, the test bench design, and the test plan establishment [2].

2.1. Flexures design

The novel flexures designed in this project were so called double blades with lattice features. As illustrated in Fig. 3, the double blade is composed of a *master* blade and a thinner *slave* blade. The master blade, which is thicker, leads the motion. Tab. 1 lists the dimensions of these flexures.

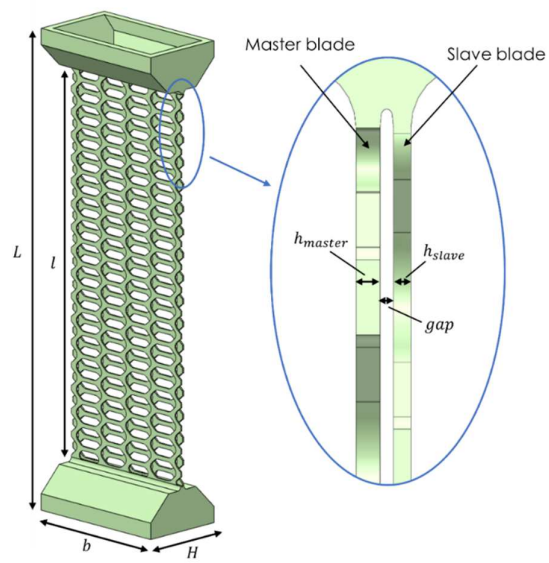

Figure 3: Elements and dimensional parameters of the flexures.

Table 1: Design parameters of the flexures

Parameter	Symbol	Value	Unit
Blade length	l	47.6	mm
Blade width	b	18.2	mm
Blade thickness (master)	h_{master}	220	µm
Blade thickness (slave)	h_{slave}	160	µm
Gap between blades	gap	125	µm
Total length (with supports)	L	58.6	mm
Total thickness (with supports)	H	10.5	mm

Two blade configurations were implemented to compare their damping performances and select the most promising geometry. In addition to the “clamped-clamped” flexure presented in Fig. 3, a “clamped-free” configuration was also designed as shown in Fig. 4. This second blade design is characterized by the release of the upper extremity of the slave blade, which is not clamped to the upper support.

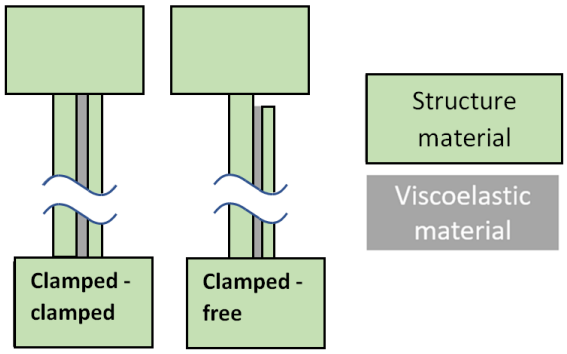

Figure 4: "Clamped-clamped" and "clamped-free" blade configurations.

Moreover, small 3D structures – called *spikes* – were added on the horizontal parts of the lattices as illustrated in Fig. 5. These aimed at increasing the strain and thus the damping in the elastomer when the flexures are bent. Configurations with and without spikes were both tested and compared (see Tab. 2) [2].

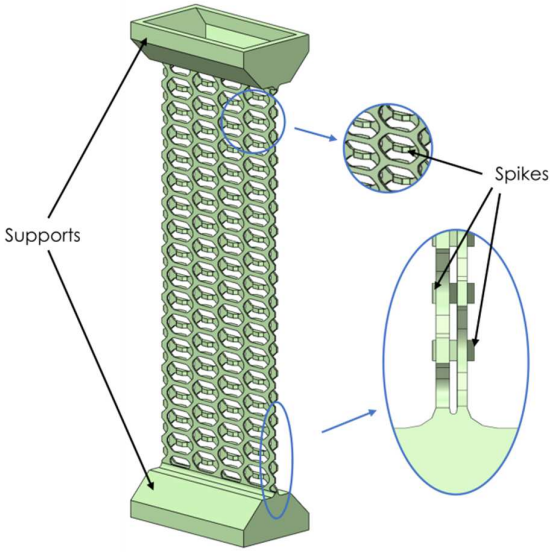

Figure 5: Flexures with spikes.

2.2. Flexures manufacturing and impregnation

The flexures were additively manufactured in 17-4PH stainless steel using a Laser Powder Bed Fusion (LPBF) process. Then, after undergoing a stress relief treatment and being removed from the build-plate, the flexures were impregnated with an elastomer. Based on a state-of-the-art search, the polyurethane acrylate UVEKOL S and the silicone Alpha gel C were selected. These two viscoelastic materials were deposited on the blades using a syringe and crosslinked using UV light. After this process, the impregnated flexures (shown in Fig. 6) were ready to be tested under vibrations [2].

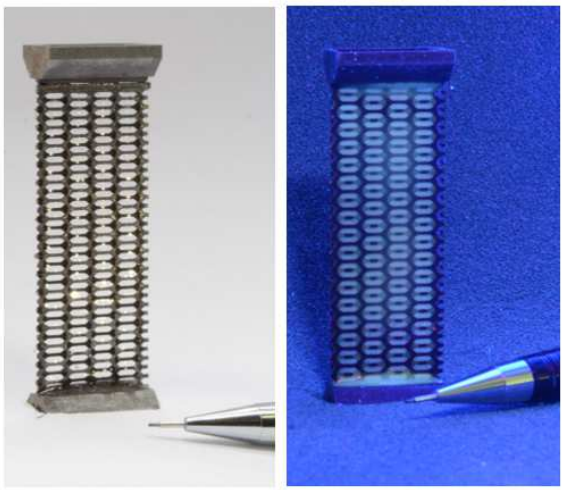

Figure 6: Final impregnated flexures (under UV light on the right).

2.3. Test bench design

Prior to starting the test campaign, a test bench, illustrated in Fig. 7, was designed to perform free oscillation tests. Two identical flexures are mounted in a parallel-spring-stage configuration on a base (violet pieces) that is fixed to a baseplate. A rotating DC motor, attached to the base, is then used to bring the moving part (yellow part) to a specific stroke. Finally, the moving part is released, and a linear encoder records its position with respect to time [2].

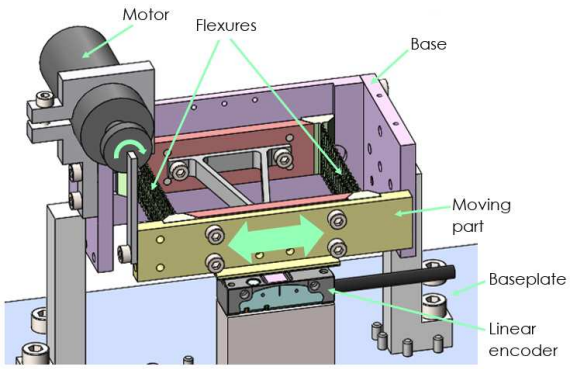

Figure 7: Test bench design.

Additionally, the test bench can be suspended to allow tests under external excitation. In this case, the bench is no more fixed to the baseplate but rather suspended using three threads and linked to a shaker through two decoupling rods as shown in Fig. 8. The DC motor is removed, and accelerometers are placed on the base and the moving part of the test bench to record their acceleration.

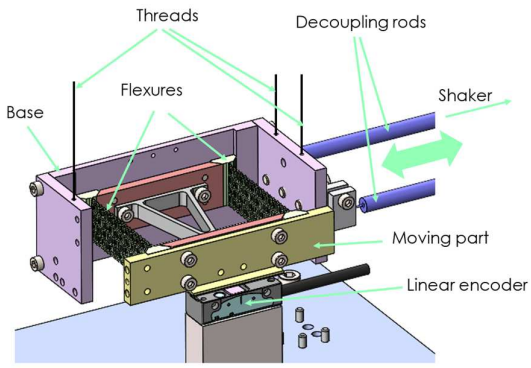

Figure 8: Suspended bench for tests under external excitation.

2.4. Test plan

2.4.1. Free oscillation test plan

The first phase of the test plan consisted in testing the different blade configurations listed in Tab. 2 in free oscillation. The reference blade is a simple – not split – blade with the same lattice pattern as the other tested flexures. However, its thickness is set to 245 µm to obtain the same stiffness and resonance frequency as the double blades. This reference allows the comparison of the impregnated double blades with the already existing state-of-the-art single blades.

Table 2: List of the tested configurations.

Blade types		Clamped-clamped	Clamped-free	Ref.
UVEKOL S *PU acrylate*	-	X	X	
	Spikes	X	X	
Alpha gel C *Silicone*	-			
	Spikes	X	X	
Without elastomer	-			X
	Spikes			

From the recorded motion of the moving part in free oscillation, curves similar to the one shown in Fig. 9 are expected. A decreasing exponential curve is then fitted to the maximum amplitude of each oscillation.

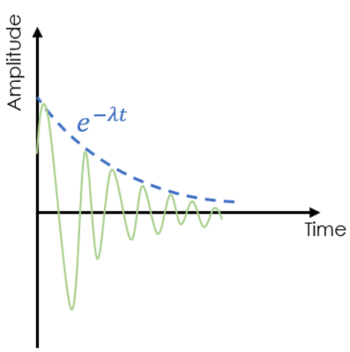

Figure 9: Typical graph obtained in a free oscillation test.

The quality factor Q and actual damping c are computed from these exponential models to assess and compare the damping performances of the different blades. Eqs. 1 and 2 are used:

$$Q = \frac{\omega_0}{2\lambda}, \qquad (1)$$

$$c = 2m\lambda, \qquad (2)$$

where $\boldsymbol{\omega_0}$ is the angular pulsation obtained from the oscillation period ($\boldsymbol{T_0}$): $\boldsymbol{\omega_0} = \boldsymbol{2\pi/T_0}$, λ is the damping coefficient obtained from the model and $\boldsymbol{m}$ the mobile mass. The smaller the quality factor is, the larger the damping is, and inversely for the actual damping [2].

2.4.2. Hysteretic damping test plan

In a second phase, the plan was to assess the different blade configurations under external excitation to obtain their hysteresis curves. A process similar to the indirect method used in [11] was followed. From the recorded acceleration of the moving part at the flexures' resonance frequency, the flexures' reaction force F can be computed according to Eq. 3:

$$F = m \cdot a \qquad (3)$$

where m is the mobile mass and a the measured acceleration. Then, the hysteresis curves which represent the force as a function of the position can be obtained. Curves as the one shown in Fig. 10 are expected.

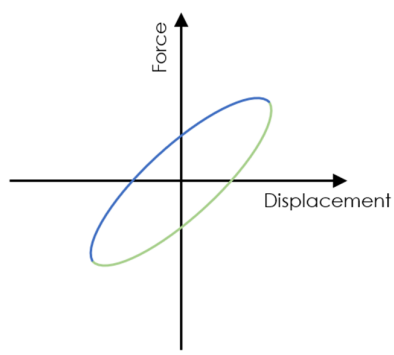

Figure 10: Typical hysteresis curve obtained under cycling displacement.

These curves allow observing the dynamic characteristic of the elastomers impregnated on the flexures. Information such as the nonlinearity of the damping along the stroke can be obtained. Additionally, comparisons of the damping data can be made with the free oscillation tests results. Indeed, in this case, the energy dissipated corresponds to the area of the hysteresis loop.

The measurement setup for the acquisition of the hysteresis curve is shown in Fig. 11. A differential measurement strategy with an accelerometer

mounted on the moving part and a second one on the base was used to compute the hysteresis curve.

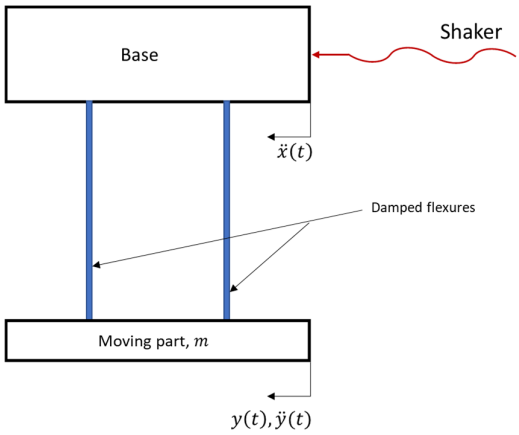

Figure 11: Schematic illustration of the measurement setup for hysteresis curve.

The dynamic of the system can be described using Eqs. 4 and 5:

$$m\ddot{y}(t) + r\dot{z}(t) + kz(t) = 0, \qquad (4)$$

$$z(t) = y(t) - x(t), \qquad (5)$$

where m is the mass of the moving part, r the viscous damping coefficient, k the rigidity and $x(t)$ and $y(t)$ the base and moving part positions respectively. The reaction force of the flexures F is equal to the sum of the viscous term $r\dot{z}(t)$ and the elastic term $kz(t)$. According to Eq. 3 and 4, F can be computed from $F = m\ddot{y}(t)$. The equivalent viscous damping ratio can be obtained from the Eq. 6 [12]:

$$\varsigma = \frac{A_h}{4\pi A_c} = \frac{A_h}{2\pi F_m D_m} \qquad (6)$$

where the dissipated energy A_h corresponds to the area covered by the hysteresis loop in Fig. 12, F_m is the maximum flexures' reaction force and D_m is the maximum amplitude of the displacement $z(t)$.

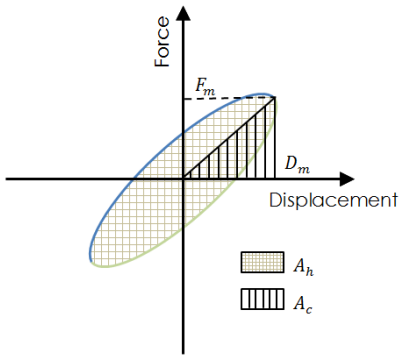

Figure 12: Hysteretic areas for equivalent viscous damping ratio determination.

The actual damping c is obtained using Eq. 7:

$$c = \varsigma c_c \qquad (7)$$

where $c_c = 2m\omega_0$ is the critical damping.

3. RESULTS AND DISCUSSION

3.1. Free oscillation tests

From the gathered data illustrated in Fig. 13, two qualitative observations are made. First, adding the elastomer greatly enhances the damping performances. Indeed, in Fig. 13, the reference continues to oscillate after hundreds of seconds while the impregnated blades stop moving after about ten seconds. Secondly, one can say that the UVEKOL S impregnated blades have higher damping performances than with Alpha gel C.

Following the exponential curve fitting on the measured time-domain datapoints, the damping parameters listed in Tab. 3 are obtained. The values mentioned in Tab. 3 are the mean values of five different free oscillation tests performed for each blade configuration.

Table 3: Results of the free oscillation tests.

Blade configuration	Elastomer	Quality factor	Actual damping
		Q [-]	c [kg/s]
Reference	-	1250.36	0.0024
Clamped-clamped	UVEKOL S	24.27	0.1981
Clamped-clamped with spikes	UVEKOL S	23.82	0.2039
	Alpha gel C	66.63	0.0472
Clamped-free	UVEKOL S	19.49	0.2339
Clamped-free with spikes	UVEKOL S	27.54	0.1677
	Alpha gel C	39.16	0.0777

These quantitative parameters confirm the observations made previously with impregnated flexures exhibiting a greatly improved damping. The quality factor Q is reduced from 18.8 to 64.2 times and the actual damping c is increased from 19.7 to 97.5 times for the impregnated blades compared to the reference.

Additionally, the UVEKOL S polyurethane acrylate shows improved damping with Q values ranging from 20 to 30, compared to the Alpha gel C having Q values of 40 and 67. The similar tendency is observed with the parameter c. The lower damping effect of the Alpha gel C comes from its gel form that makes it softer than the UVEKOL S. With the large deformations of the blades, the Alpha gel C brings

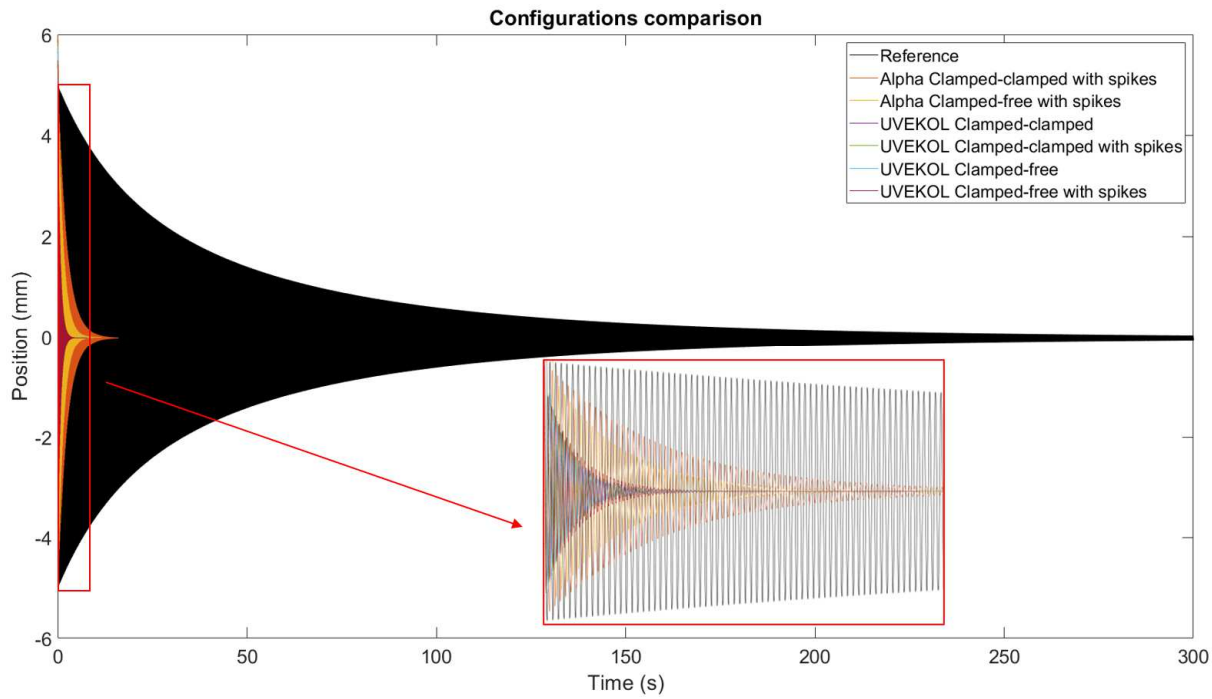

Figure 13: Free oscillation test results of all the different blade configurations.

lower damping to the blades than UVEKOL S. Thus, this latter is more interesting for the present application.

Concerning the geometry of the flexures, the most promising blade configuration to increase the damping effect is clamped-free with UVEKOL S. The spikes do not seem to improve the damping of the flexures. These lower performances could be explained as, in these configurations, less elastomer is impregnated between the blades as the spikes locally fill the gap. Since less elastomer induces less energy stored in and dissipated, this results in a reduced damping of the blade motion. Moreover, the clamped-free configuration shows a higher damping than the clamped-clamped configuration. This improved performance of the clamped-free configuration is due to its free end not being directly linked to the motion of the moving part. The motion transmission to this free end is only made by the elastomer, causing it to deflect more. More stress is synonymous with more energy dissipated in the elastomer which finally induces more damping of the blade motion [2].

3.2. Statistical modelling

A data analysis was performed to identify the effects of different factors on the resulting damping. The elastomer material, the blade fixation type ("clamped-clamped" or "clamped-free") and orientation with respect to gravity are considered as experimental factors. A fourth factor is used to analyse whether the test method has an influence on the measured damping. Two additional test methods using the suspended test bench configuration (see section 2.3) and frequency-domain damping evaluation methods are considered. This factor should ideally not influence the obtained result. A constant coefficient model can be employed to model the data. The structure of Eq. 8 can be used:

$$y = \mu + \alpha_e + \beta_b + \gamma_o + \delta_t + \varepsilon, \qquad (8)$$

with μ being the grand mean representing an intercept term, α_e, β_b, γ_o, δ_t representing the residuals for the elastomer material, the blade fixation, the orientation, and the test type, respectively, ε corresponds to the residuals and y to the resulting damping.

Employing an analysis of variance (ANOVA), it can be determined whether the mean values of several groups differ statistically significantly. The hypothesis for the ANOVA can be formulated as follows for each of the factors:

- h_0: The factor has no influence on the damping properties of the flexure.
- h_1: The factor has an influence on the damping properties of the flexure.

The null hypothesis h_0 can then be rejected or accepted at a certain p-value. This value represents the probability that the effect is obtained by chance, which means that a lower p-value indicates higher significance of the factor under test. For this study, a significance level of p = 0.05 is defined.

For many statistical analysis tools, such as ANOVA, it is assumed that the prediction errors (residuals) come from a normally distributed population. Fig. 14 shows the residuals and Fig. 15 the normal plot of the residuals. Fig. 14 reveals that the residuals are randomly dispersed around the horizontal axis, which indicates that a linear regression model is appropriate to fit the data.

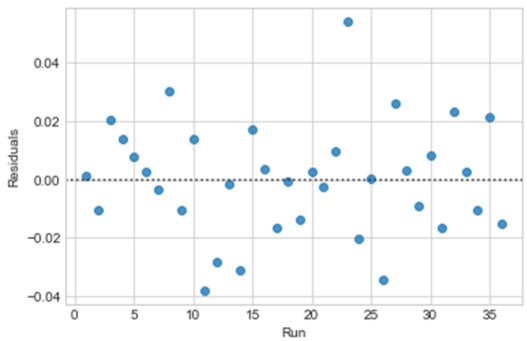

Figure 14: Residual plot.

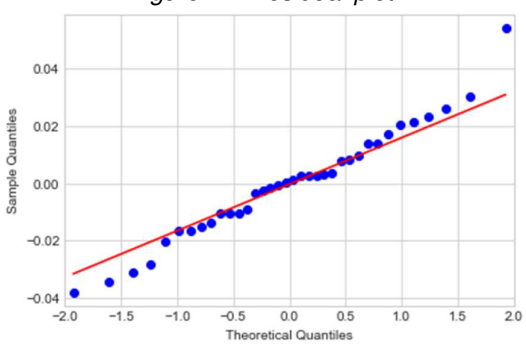

Figure 15: Normal plot of the residuals.

The normal plot (or quantile-quantile plot) in Fig. 15 indicates a normal distribution with the residuals following a linear function in good approximation. For a quantitative assessment, a Shapiro-Wilk test was employed, which reveals a p-value of p = 0.783. Based on this p-value the null-hypothesis, h_0: The underlying population of the sample is normally distributed, can be accepted at a significance level of 0.05. These results support the assumption that the data is normally distributed, and an ANOVA can be performed. The resulting ANOVA is presented in Tab. 4.

Table 4: ANOVA table for the constant coefficient model; F representing a theoretical distribution (Fisher) and PR(>F) the corresponding p-value.

	F	PR(>F)
Intercept	35.1913	1.918e-06
Elastomer material	360.4587	3.289e-21
Blade fixation	6.3087	1.783e-02
Orientation	18.8719	1.560e-04
Evaluation test	0.6189	5.455e-01
Residual	NaN	NaN

A calculated p-value below the critical value of p = 0.05 indicates that a factor has an influence on the damping. Tab. 4 reveals that the elastomer material has the largest influence on the damping, followed by the orientation as well as the blade fixation. The influence of the test type on the damping can be assessed as low.

The high influence of the elastomer material on the damping properties of the flexures is expected from the qualitative analysis and is confirmed by the computed effects presented in Fig. 16. The impregnated layer of an elastomeric material is adding damping properties to standard flexures and the material properties of the elastomer will greatly influence the value of the achieved damping. A careful selection of the elastomer to apply is therefore crucial.

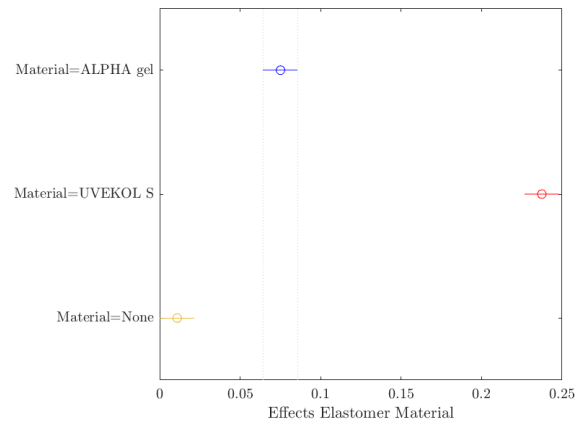

Figure 16: Computed effects α_e for the elastomer material.

The second most important factor, even if significantly less important compared to the material choice, is the blade fixation. Depending on the mechanical fixation, different forces and torques are applied, thereby influencing the dynamics of the blades. From the experimental data, the clamped-free configuration leads overall to the best performance as can be seen from the computed effects given in Fig. 17.

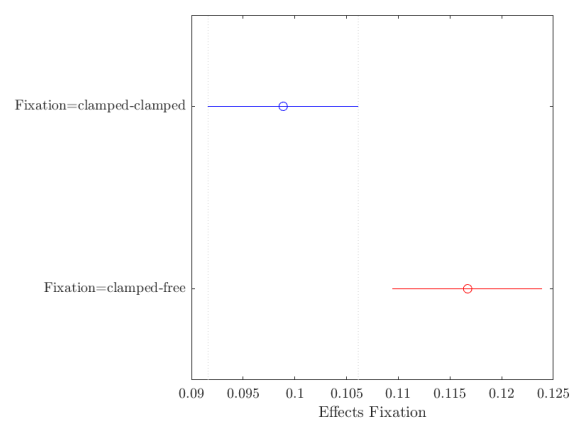

Figure 17: Computed effects β_b for the blade fixation.

The orientation of the blades with respect to the gravity is almost as important as the blade fixation as shown in Fig. 18. This can be problematic when using the damped flexures for instance in a vibration isolation system. The orientation of the flexures will typically be a free choice of the user and the attenuation properties of the system should ideally be the same for all orientations. Further investigations should be made to evaluate the source of this effect more closely and to identify possible solutions.

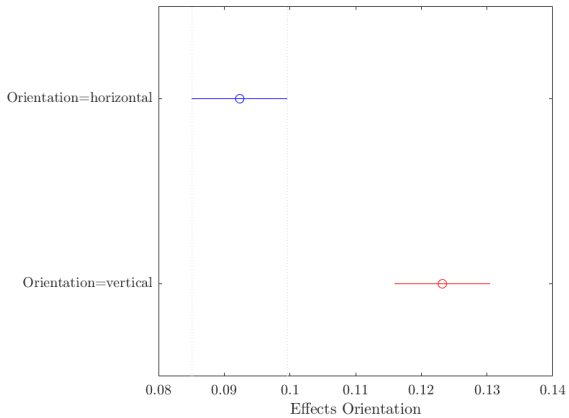

Figure 18: Computed effects γ_o for the orientation with respect to the gravity.

Regarding the evaluation method, no significant difference between the methods could be found as can be seen from Fig. 19. This is an expected result as the evaluation method should not influence the obtained result.

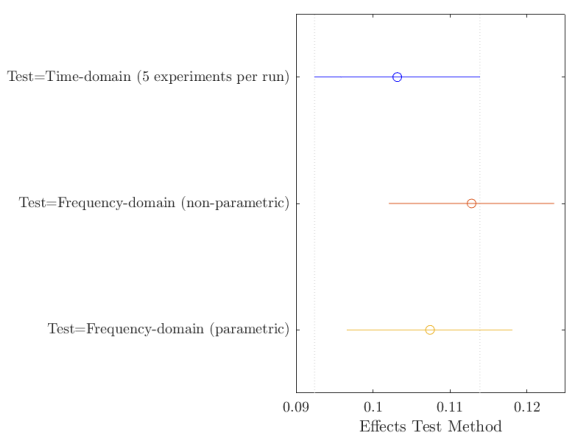

Figure 19: Computed effects δ_t for the different test methods.

3.3. Hysteretic damping tests

In addition to their characterization in free oscillation, the flexures were also tested under external excitation. The obtained data show similar damping performances for the impregnated blades and confirm the results obtained in free oscillation. From these supplementary tests, hysteresis curves were also obtained as shown in Fig. 20.

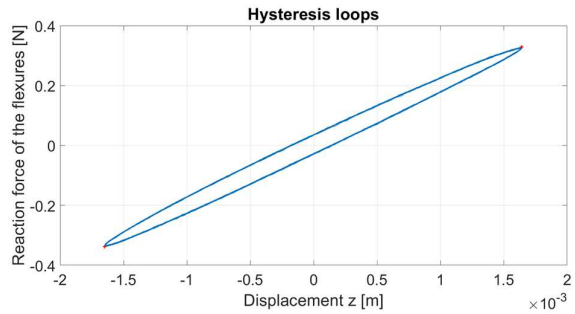

Figure 20: Resulting hysteresis curve.

A single hysteretic damping curve provides information about the damping behaviour of a system under cyclic loading. From a single damping curve, it is possible to analyse the following properties:

- **Damping ratio:** The damping ratio indicates the proportion of energy that is lost in a single cycle of loading. The damping ratio can be calculated from the hysteretic damping curve as the ratio of the energy dissipated in one cycle to the energy stored in the system during that cycle. These energies correspond respectively to the areas A_h and A_c in the Fig. 12 and the damping ratio can be computed according to Eq. 6.
- **Energy dissipation rate:** The energy dissipation rate can be determined from the hysteretic damping curve by calculating the rate of change of the energy dissipated in each cycle of loading. The hysteresis loops shown in Fig. 20 are obtained for 100 cycles of loading and are all very similar. The obtained dissipation rate is therefore small for 100 cycles of loading.
- **Cyclic loading behaviour:** The hysteretic damping curve can provide information about the system's behaviour under cyclic loading, such as its stability and its tendency to undergo fatigue or other types of degradation. For an absolute displacement smaller than 1 mm, Fig. 20 shows a linear behaviour of the flexures regarding the displacement. Moreover, for 100 cyclic loadings, the damping system shows a certain consistency in its behaviour as all the hysteresis loops are almost superimposed.
- **Material properties:** The damping behaviour of a system is influenced by its yield strength, and toughness. By analysing the hysteretic damping curve, it is possible to estimate some of these material properties such as its elastic modulus.

However, it is worth noting that the information that can be obtained from a single hysteretic damping

curve is limited. To gain a more comprehensive understanding of a system's properties, it is often necessary to analyse multiple hysteretic damping curves taken under different conditions or using different loading methods.

4. CONCLUSION AND OUTLOOK

The present article detailed the complete process of the development, manufacturing and testing of a novel damping technology consisting in elastomer-impregnated flexures. These newly developed flexures exhibit greatly improved damping performances with **a quality factor reduction of up to 64 times** and **an actual damping increased by up to 97 times** compared to reference simple flexure blades. Therefore, the impregnated lattice blades produced are an innovative solution to withstand vibrations and shocks [2].

In addition to these blades, the impregnation process could also be applied to other flexure types (see Fig. 21). A wide range of different flexures are available and can be combined to obtain the specific desired motion. They could then represent an alternative way to design state-of-the-art spring dampers. Indeed, they could be used to minimize exported vibrations of a variety of sources such as cryo-coolers or reaction wheels in satellites. Reversely the vibration susceptibility of systems such as metrology instruments, optical setups and industrial vision systems could be reduced thanks to a decoupling from the surrounding environment. Fig. 21 illustrates some examples of the flexures toolbox elements that could be impregnated and then combined to allow specified motion and damping of the desired structure.

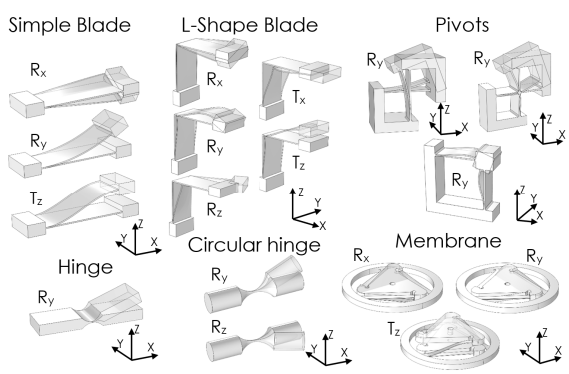

Figure 21: Examples of the flexures toolbox elements.

These flexures damping could even be tuned to act at specific frequencies by a right tailoring of their physical parameters. Moreover, this passive damping elements could be combined with an active damping system to adjust at best to the desired application.

From this research, several topics could be further investigated in the future:

- **Impregnated flexures modelling:** Developing a model will allow predicting the damping performance of the flexures during the design phase, thus facilitating the tailoring of the flexures' geometry and the choice of the elastomeric material for a specific application.
- **Further testing:** Tests under forced oscillation with varying excitation frequencies (sine sweep) were conducted, but without conclusive results in some cases due to a limited position sensor resolution. Those shall be repeated after having improved the test bench. Additional characterization such as fatigue tests is necessary to assess the flexure performance during its complete lifetime. Behaviour at different temperatures or under vacuum would also be interesting to study in order to analyse the elastomer ageing phenomenon as well as its damping behaviour with changing conditions [2].

5. ACKNOWLEDGMENT

This project was carried out as part of a Master's thesis and under the supervision of Loïc Tissot-Daguette, Florent Cosandier and Prof. Simon Henein of the EPFL Instant-Lab which we would like to thank.

6. REFERENCES

1. Smet, G. & Patti, S. (2018, May). A Mechanisms Perspective on Microvibration–Good Practices and Lessons Learned. In *44th Aerospace Mechanisms Symposium* (p. 191).
2. Salamin, L., Saudan, H., Cosandier, F., Kiener, L., Klauser, E., Blondiaux, N., Boudoire, F., Kalentics, N., Tissot-Daguette, L. & Henein, S. (2023). Damping of flexure blades based on bi-material additive manufacturing. [Manuscript submitted for publication]. euspen.
3. Spanoudakis, P., Schwab, P., Kiener, L., Saudan, H. & Perruchoud, G. (2015, September). Development Challenges of Utilizing a Corner Cube Mechanism Design with Successful IASI Flight Heritage for the Infrared Sounder (IRS) on MTG; Recurrent Mechanical Design Not Correlated to Recurrent Development. In *16th European Space Mechanisms and Tribology Symposium*.
4. Cosandier, F., Henein, S., Richard, M. & Rubbert, L. (2017). *The art of flexure mechanism design* (No. BOOK). Epfl Press.
5. Ahn, D. G. (2016). Direct metal additive manufacturing processes and their sustainable applications for green technology: A review. *International Journal of Precision Engineering and Manufacturing-Green Technology*, *3*, 381-395.
6. Kiener, L., Saudan, H., Cosandier, F., Perruchoud, G., Ummel, A., Pejchal, V., Zaltron, P., Puyol, Y. & Lichtenberger, M. (2021). Compliant mechanism based on additive

manufacturing. *CEAS Space Journal*, 1-17.
7. Spanoudakis, P., Schwab, P., Kiener, L., Perruchoud, G., Saudan, H., Gumy, M. & Regamey, Y. J. (2019). Corner Cube Mechanism (CCM) for MTG IRS: qualification and acceptance test campaign results and lessons learned. *Proceedings of the 18th ESMATS*.
8. Bustamante, M., Gerges, S. N., Vergara, E. F. & Arenas, J. P. (2016). High damping characteristics of an elastomer particle damper. *International Journal of Acoustics and Vibration*, *21*(1), 112-121.
9. Frankovich, D. (2000). *The basics of vibration isolation using elastomeric materials*. Society of Manufacturing Engineers.
10. Droz, S., Musy, G., Dominé, E. & Barrot, F. (2016). *Damping device, in particular for micromechanical clock component* (CH Patent No. EP3076245A1)
11. Petrone, F., Lacagnina, M. & Scionti, M. (2004). Dynamic characterization of elastomers and identification with rheological models. *Journal of Sound and Vibration*, *271*(1-2), 339-363.
12. Priestley, M. N., Seible, F. & Calvi, G. M. (1996). *Seismic design and retrofit of bridges*. John Wiley & Sons.